ACS NANO
Cite This: ACS Nano XXXX, XXX, XXX–XXX
www.acsnano.org

ARTICLE

High-Pressure Effect on the Optical Extinction of a Single Gold Nanoparticle

Fabio Medeghini, Mike Hettich,[†] Romain Rouxel, Silvio D. Silva Santos, Sylvain Hermelin, Etienne Pertreux, Abraao Torres Dias,[‡] Franck Legrand,[§] Paolo Maioli, Aurélien Crut, Fabrice Vallée, Alfonso San Miguel, and Natalia Del Fatti*

Université de Lyon, CNRS, Université Claude Bernard Lyon 1, Institut Lumière Matière, 69622 Villeurbanne Cedex, France

Supporting Information

ABSTRACT: When reducing the size of a material from bulk down to nanoscale, the enhanced surface-to-volume ratio and the presence of interfaces make the properties of nano-objects very sensitive not only to confinement effects but also to their local environment. In the optical domain, the latter dependence can be exploited to tune the plasmonic response of metal nanoparticles by controlling their surroundings, notably applying high pressures. To date, only a few optical absorption experiments have demonstrated this feasibility, on ensembles of metal nanoparticles in a diamond anvil cell. Here, we report a nontrivial combination between a spatial modulation spectroscopy microscope and an ultraflat diamond anvil cell, allowing us to quantitatively investigate the high-pressure optical extinction spectrum of an individual nano-object. A large tuning of the surface plasmon resonance of a gold nanobipyramid is experimentally demonstrated up to 10 GPa, in quantitative agreement with finite-element simulations and an analytical model disentangling the impact of metal and local environment dielectric modifications. High-pressure optical characterizations of single nanoparticles allow for the accurate investigation and modeling of size, strain, and environment effects on physical properties of nano-objects and also enable fine-tuned applications in nanocomposites, nanoelectromechanical systems, or nanosensing devices.

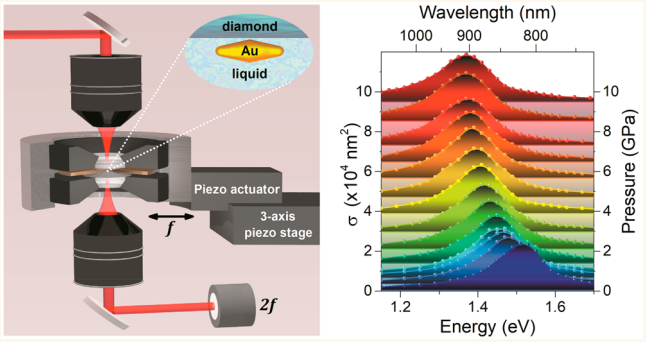

KEYWORDS: *single nanoparticle extinction, spatial modulation spectroscopy, high pressure, diamond anvil cell, surface plasmon resonance, gold bipyramids*

The electromagnetic response of metal nano-objects is dominated by localized surface plasmon resonances (LSPR) enhancing their optical absorption and scattering at specific wavelengths.[1,2] Because of their large fundamental and technological interests, plasmonic properties have been extensively investigated both experimentally and theoretically during the past decades, on ensembles and more recently at the single-particle level.[3−6] The LSPR tunability with the nano-object size, shape, composition, and surrounding environment (e.g., a solid matrix, a liquid, a substrate, molecules, or other nanoparticles) has been continuously improved following the development of new design and production methods,[7−9] concomitant with detailed modeling for the understanding of the physical mechanisms at the origin of linear and ultrafast plasmonic responses.[10] In particular, elongated nanoparticles such as gold nanobipyramids (Au-BPs) exhibit a sharp longitudinal resonance in the visible and near-infrared spectral domain, adjustable by modifying either their aspect ratio or local environment.[11−14] The high sensitivity to the latter is enhanced around the tips of BPs, making them very suitable for nanosensing applications.[15,16] In this context, a way to continuously tune the optical properties of a nanomaterial is to subject it, and its environment, to high-pressure conditions.[17−21] The first optical extinction spectra, in the 0−10 GPa range, were measured on ensembles of metal nanoparticles in glass or water−ice.[22−25] These experiments employed a diamond anvil cell (DAC) apparatus generating a tunable hydrostatic high-pressure environment up to hundreds of gigapascals when reducing the distance between two diamond anvils separated by a pressure-transmitting medium (e.g., a transparent fluid).[26,27] A spectral shift in the sample absorption and irreversible processes were highlighted. However, in such ensemble experiments, the unavoidable size and shape dispersion of investigated nano-objects precluded a precise characterization and modeling of the pressure-dependent optical response. In particular, they did not

Received: July 23, 2018
Accepted: October 5, 2018

DOI: 10.1021/acsnano.8b05539
ACS Nano XXXX, XXX, XXX–XXX

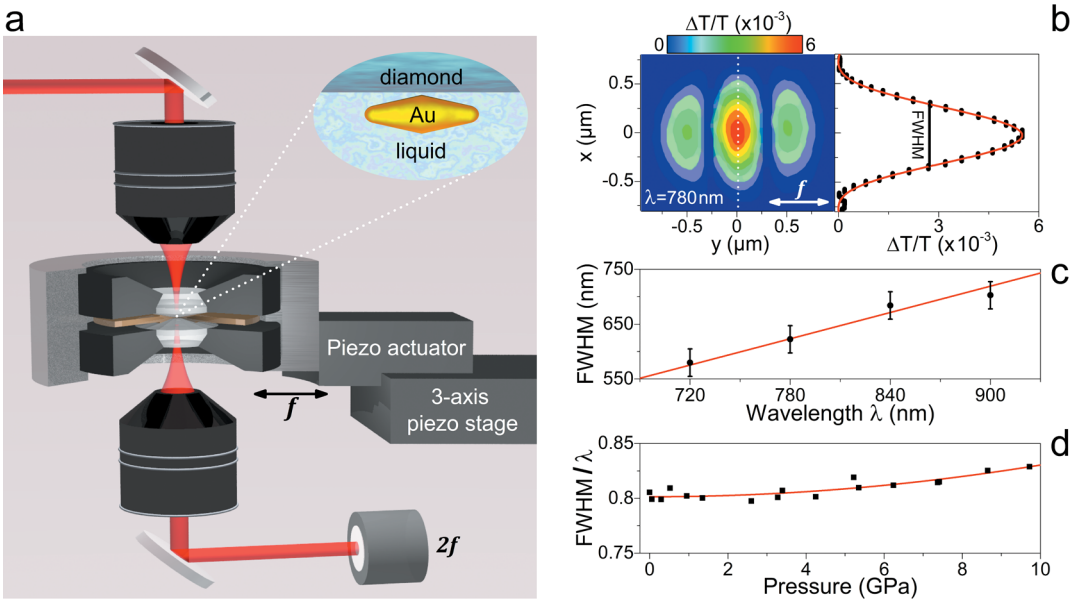

Figure 1. Optical extinction of a single nano-object under high pressure. (a) Developed experimental setup, involving the combination of an ultraflat DAC with a SMS microscope. Quantitative extinction measurements were performed on Au-BPs spin-coated on the upper diamond and immersed in a liquid pressure-transmitting medium (4Me:1Et). SMS consists of modulation of the sample position under a focused laser beam, using a piezoelectric actuator driven at frequency f, with synchronous detection at $2f$ of the induced relative transmission changes, $\Delta T/T$, proportional to the nanoparticle extinction cross section. Images are acquired by sample scanning using a piezoelectric stage. (b) SMS image of a single Au-BP at λ = 780 nm illumination wavelength, consisting of three lobes along the modulation direction y, as a result of the modulation process. The $\Delta T/T$ profile along direction x orthogonal to the modulation one (white dotted line) shows the focused beam intensity, fitted by an Airy function of full-width at half-maximum (fwhm) (red line). (c) Wavelength dependence of fwhm (black dots) measured at low pressure (P = 0.06 GPa) and linear fit (red line). (d) Measured pressure dependence of the fwhm/λ ratio (black squares), close to diffraction-limit and with weak pressure parabolic variations (red line fit).

allow the quantitative attribution of the observed pressure effects to intrinsic or extrinsic (i.e., related to metal or environment modifications, respectively) contributions.

Optically addressing *in situ* a single nano-object in a DAC is very challenging and represents a major step toward quantitative investigation and control of material properties at the nanoscale. Characterization of morphology and strain evolution of individual metal particles (Au 400 nm and Ag 120 nm size cubes) in a DAC was recently achieved by coherent X-ray diffraction imaging.[28,29] Optical trapping of a large (micrometer size) single dielectric particle was also demonstrated in a DAC, permitting local measurements of water viscosity.[30] Here, we report a quantitative high-pressure study of the optical extinction of a single metal nanoparticle in a DAC, made possible by designing a specific setup based on spatial modulation spectroscopy (SMS). SMS is a highly sensitive far-field optical technique that yields the absolute extinction cross-section, $\sigma(\omega)$ (sum of the absorbed and scattered electromagnetic powers divided by the incident intensity), of an individual nano-object as a function of the illuminating light frequency (ω) and polarization angle.[31,32] It allows investigations of a large variety of nano-objects, including metal nanoparticles down to 2 nm size, single-wall carbon nanotubes, semiconductor nanowires, and nano-tips.[3,33−35] Single-particle optical microscopy at high pressure was achieved here by periodically modulating the spatial position of a designed ultraflat DAC, containing individual Au-BPs. Development of this challenging setup allowed us to experimentally monitor the evolution of the nanoparticle spectrum in the visible to near-infrared range. This spectral response is dominated by the metal LSPR and undergoes a pronounced nonlinear red-shift in the 0−10 GPa pressure range. In contrast to ensemble measurements, these pressure-adjustable plasmonic changes at the nanoscale are here quantitatively reproduced by an analytical model and optical finite-element simulations that take into account the actual nanoparticle morphology and its inhomogeneous environment. This elucidates the physical mechanisms at the origin of LSPR spectral modifications, showing the impact of both metal and environment dielectric function pressure-induced changes.

RESULTS AND DISCUSSION

To enable optical detection and quantitative extinction cross-section measurements of a single nano-object under high pressure, an ultraflat membrane DAC was specifically designed and realized for experiments under hydrostatic pressure in the 0−10 GPa range (Figure 1a; see also Methods and Figure S1 of the Supporting Information for details). This was combined with a SMS microscope, which relies on illumination of a single nanoparticle with a tightly focused laser beam and direct detection of the transmitted light. Single-particle sensitivity is achieved by mechanical modulation (at frequency f) of the sample position under the focal spot, and synchronous detection (at frequency f or $2f$) of the induced relative changes in the transmitted light, $\Delta T/T$, by a photodiode and lock-in amplifier. High sensitivity, $(\Delta T/T)_{min} \approx 10^{-5}$, is attained with modulation frequencies f in the kilohertz range, oscillation amplitudes δ of the order of the focal spot size, and close to diffraction limit illumination with high stability lasers, allowing detection of individual nano-objects with extinction cross sections down to σ_{min} of a few square nanometers.[31]

For high-pressure SMS experiments with a DAC, the entire DAC containing the nanoparticles was fixed on the mobile part

DOI: 10.1021/acsnano.8b05539
ACS Nano XXXX, XXX, XXX−XXX

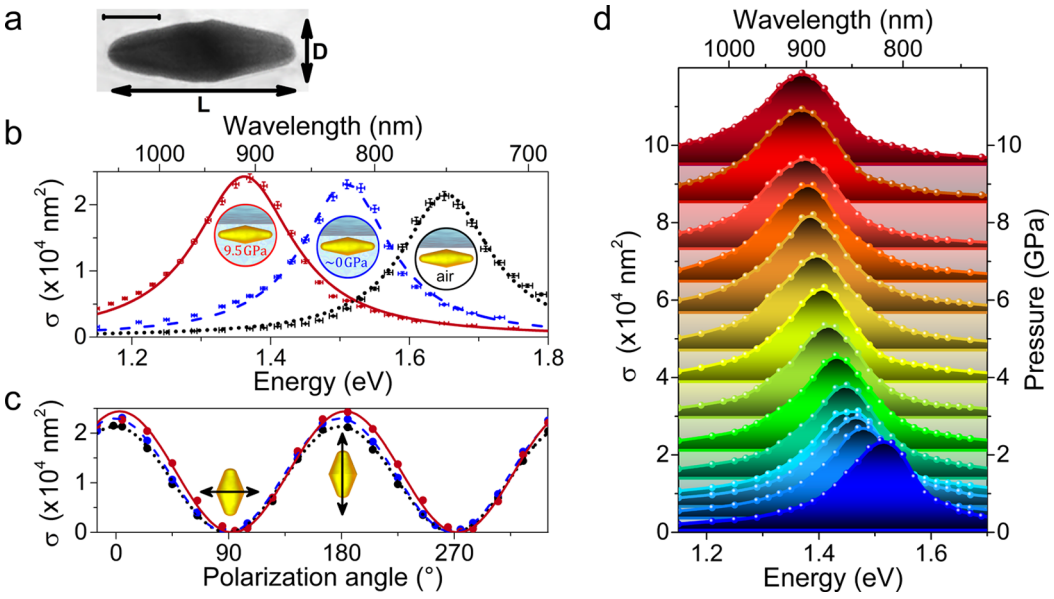

Figure 2. Quantitative LSPR spectra of a single Au-BP under high pressure. (a) TEM image of a Au-BP from the colloidal solution with 93 × 33 nm mean size (scale bar, 30 nm).[11,12] (b) Extinction cross section (σ) spectra (dots, SMS measurements; lines, Lorentzian fits) of a single Au-BP deposited on diamond in air at P_0 = 0 GPa (black) and in the 4Me:1Et pressure-transmitting liquid at low (P = 0.06 GPa, blue) and high (P = 9.5 GPa, red) pressures, for light polarization parallel to the BP major axis. (c) σ-polarization dependence in these three configurations, measured at the LSPR wavelength (dots, SMS measurements; lines, sinusoidal fits). (d) Au-BP extinction cross-section spectra (left axis), vertically shifted for clarity, measured at increasing pressures (right axis).

of a uniaxial piezoelectric actuator (inducing the spatial modulation along the y axis), whose base was mounted on the top of a 3-axes piezoelectric stage for sample position scanning (Figure 1a). Because of the weight of the sample, its mechanical movement at high frequency was challenging. The ensemble composed by the DAC and the two piezoelectric components behaves like a system of coupled oscillators, whose complete mechanical characterization was performed to achieve appropriate working conditions, f = 940 Hz and δ = 600 nm. The illuminating source is a femtosecond-pulsed Ti:sapphire oscillator tunable in the λ = 680−1080 nm wavelength range. It was focused on the inner surface of the diamond anvil by a tailored 100× precompensated microscope objective (Mitutoyo, 0.7 numerical aperture, 1 cm working distance), which was specifically designed to minimize the aberrations produced by the passage of the light through the 1.4 mm thick diamond anvil. Note that use of a non-compensated microscope objective of the same specifications yielded a beam with severe aberrations, precluding any SMS investigation of a single nano-object in the DAC.

Optical extinction spectroscopy was performed on individual gold bipyramids (Au-BPs) spin-coated on the inner face of one of the two diamonds constituting the DAC (inset of Figure 1a), with a density less than one particle per square micrometer as required for far-field optical experiments on single particles. Au-BPs are nanoparticles whose chemical synthesis in colloidal solution, optical characterization at single-particle level, and modeling have been mastered in the past decade.[11−13] Nanoparticles located far from the border of the DAC gasket hole were imaged by x−y scanning the central part (∼70 μm diameter) of the diamond culet. For 2f synchronous detection, every nano-object induces a demodulated extinction signal in transmission, $\Delta T/T(x,y)$, of three lobes along the y vibration direction, where the particle position coincides with the center of the main lobe (Figure 1b). For nanoparticles smaller than the focal spot, the SMS signal along the direction perpendicular to the vibration (dotted line in Figure 1b) reproduces the intensity profile of the focused beam. The full-width at half-maximum (fwhm) beam spot size focused with the compensated microscope objective was then characterized as a function of the wavelength λ, yielding fwhm ≈ 0.8λ, close to the diffraction limit (0.73λ in air) in the whole 0−10 GPa range (Figure 1c,d). Knowledge of fwhm and oscillation amplitude permits quantitative extraction of the nano-object cross-section at the illuminating wavelength, $\sigma(\lambda)$, from the amplitude of the detected signal $\Delta T/T$.[3]

A transmission electron microscopy (TEM) image of a Au-BP is shown in Figure 2a, the geometry being characterized by its aspect ratio $\eta = L/D$, with long axis L and short axis D. Optical studies were realized at room temperature on single nanoparticles directly spin-coated from their initial aqueous solution with mean sizes $\langle L\rangle$ = 93 nm and $\langle D\rangle$ = 33 nm (5% standard deviation). The experimental spectrum of an individual Au-BP on diamond measured by SMS at standard pressure in air (P_0 ≈ 0 GPa) is shown in Figure 2b for light linearly polarized along its long axis (black points). For such elongated nano-objects, the longitudinal LSPR is located at a characteristic energy position $E_R = \hbar\Omega_R$ (or peak wavelength $\lambda_R = 2\pi c/\Omega_R$) far from the gold interband transitions (occurring below λ_R ≈ 520 nm) and thus described by a quasi-Lorentzian symmetric profile (dotted black line).[13] The strong plasmonic dependence on light polarization is highlighted in Figure 2c (black dots and dotted line). The amplitude of extinction cross-section at λ_R = 750 nm displays a sinusoidal behavior with the incident polarization angle and vanishes for light polarized along the short axis (a transverse LSPR then appears close to λ_{ib}, not shown here).[3] The response of the same Au-BP was then characterized after loading the DAC with a liquid pressure-transmitting medium, a

DOI: 10.1021/acsnano.8b05539
ACS Nano XXXX, XXX, XXX−XXX

4:1 methanol−ethanol (4Me:1Et) mixture (Figure 2b, blue points and dashed line at P = 0.06 GPa in liquid environment). This induces a LSPR spectral red-shift (λ_R from 750 nm in air to 820 nm in liquid) underlying the high sensitivity of such nano-objects to modifications of the local environment on a distance of the order of their tip size.[16] The polarization dependence shows, however, the same angular variations as in air, indicating that the orientation of the nano-object, bound to the diamond substrate, remains unchanged (Figure 2c, blue dots and dashed line). The optical extinction spectrum of the Au-BP was then measured by SMS under increasing pressure (Methods), which induces a further distinct red-shift visible in Figure 2b (λ_R from 820 to 910 nm at P = 9.5 GPa, red points and solid line). The evolution of the single-particle spectra measured in the full 0−10 GPa range is shown in Figure 2d, where each experimental curve has been shifted upward by an amount corresponding to the applied pressure (right axis). Again, the polarization dependence of $\sigma(\Omega_R)$ remains unchanged during the pressure ramp, signifying no reorientation of the particle (as shown in Figure 2c at P = 9.5 GPa, red dots and solid line).

The LSPR energy positions $E_R(P)$ of the investigated Au-BP under each applied pressure are shown in Figure 3. The resonance exhibits a nonlinear pressure-induced red-shift (black squares in Figure 3c, with $\Delta E_R \approx -150$ meV at 10 GPa corresponding to a 10% LSPR spectral detuning). A LSPR broadening under high pressure is also observed; however, its detailed investigation and determination of its physical origin require further experiments and are outside the scope of this paper. To quantitatively analyze the effect of pressure on the LSPR spectral position, we developed a complete electromagnetic finite-element method (FEM) simulation computing the extinction cross-section of the illuminated nanoparticle in its inhomogeneous environment under high pressure (Methods). The actual geometry of the experiment was taken into account (i.e., gold bipyramid deposited on the diamond substrate immersed in the pressure-transmitting liquid, Figure 3a). The Au-BP elastic deformation under hydrostatic pressure was modeled by reducing its volume $V(P)$ at constant aspect ratio using the Vinet gold equation of state (Methods).[36,37] The nanoparticle material was characterized by the complex gold dielectric function, $\varepsilon(\omega)$, which can be separated into intraband (Drude) and interband electronic contributions.[38] At the investigated optical frequencies, far from the gold interband transitions, the main pressure dependence is expected to stem from modifications of the Drude term describing the electromagnetic response of the N conduction electrons of the Au-BP (Methods). In particular, their plasma frequency ω_P, proportional to the square root of the conduction electron density $N/V(P)$, is directly affected by the nanoparticle volume compression. The diamond substrate was characterized by its real dielectric constant, ε_d, which exhibits a negligible pressure dependence.[39] The significant pressure variations (1 order of magnitude larger than the diamond ones) of the methanol−ethanol liquid dielectric constant $\varepsilon_l(P)$ were extracted from the literature.[40] LSPR spectral positions predicted from these FEM simulations are shown in Figure 3c (solid green line; see Figure S2 for complementary analysis). A very good quantitative agreement with the single-particle experimental data is achieved here (both on the absolute energy values and their nonlinear pressure evolution), demonstrating that the main physical

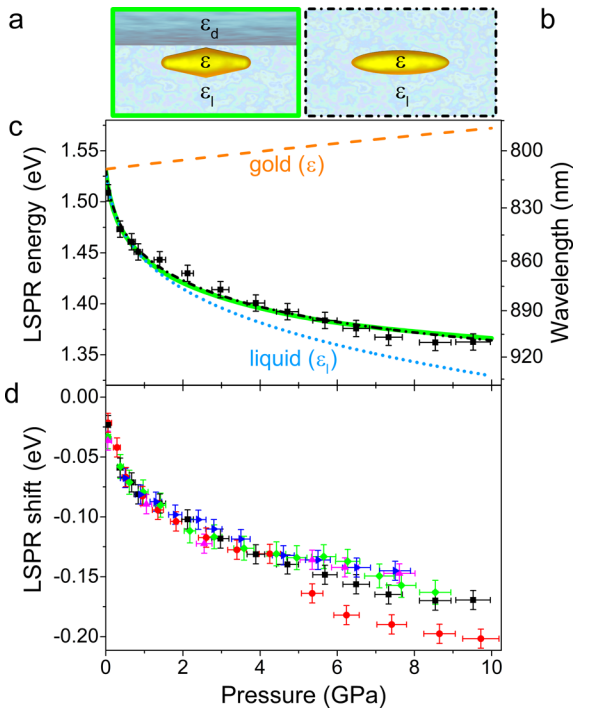

Figure 3. Pressure-induced red-shift of the LSPR of individual Au-BPs. Schematics show the configurations considered in the models: (a) Complete FEM model: Au-BP (dielectric function ε) of aspect ratio η = 3 and short axis D = 30 nm, deposited on a diamond substrate (dielectric function ε_d) immersed in pressure-transmitting liquid (dielectric function ε_l). (b) Simplified semi-analytical model: Au nanoellipsoid in a homogeneous liquid environment. (c) Measured pressure−dependence of a single Au-BP LSPR spectral position (black squares), with computations from FEM and semianalytical models (overlapped green solid and black dash−dotted lines). The shifts deduced from the simplified model by taking into account only the pressure-induced modification of ε_l (blue dotted line) or of ε (orange dashed line) are also shown (same results can be computed using the complete FEM model). (d) Pressure-induced LSPR red-shift measured on five different Au-BPs. This shift was reversible for four of them (black squares, green diamonds, magenta upward triangles, and blue rightward triangles) and irreversible for one (red dots), which showed a discontinuity above 4 GPa pressure (additional analyses in Figures S2 and S3).

phenomena at the origin of the plasmonic pressure tuning originate from the above-described dependencies.

A simplified semianalytical model based on a simpler geometry was developed, which captures the mechanisms dominating the pressure-induced variations and enables us to easily distinguish contributions from metal or environment property changes. We modeled the Au-BP as an elongated prolate nanoellipsoid embedded in a homogeneous matrix of dielectric function $\varepsilon_l(P)$, with an effective fixed aspect ratio chosen to reproduce the LSPR position at ambient pressure (Figure 3b and Methods). In the framework of the quasi-static approximation, suitable for the sizes and aspect ratios investigated here, the LSPR position is given by an analytical formula,[3] $\Omega_R(P) = \omega_P(P)/\sqrt{\tilde{\varepsilon}_1^{ib} + H\varepsilon_l(P)}$, where $\tilde{\varepsilon}_1^{ib}$ is related to the interband component of the gold real dielectric function at the resonance frequency and H is a geometrical factor depending on the Au-BP aspect ratio (Methods). The pressure-induced shift predicted by this simplified approach

DOI: 10.1021/acsnano.8b05539
ACS Nano XXXX, XXX, XXX−XXX

is in quantitative agreement with experimental data (Figure 3c, dash-dotted black line), also perfectly overlapping results from complete FEM simulations. Taking into account only variations of the liquid environment surrounding the nanoparticle (i.e., only modifying, in the denominator of the previous expression, the liquid refractive index under high pressure, ∼20% increase at 10 GPa)[40] would yield an overestimation of the plasmonic spectral shift (Figure 3c, blue dotted line). The difference is an additional blue-shift that shows the impact of modifications of the metal nanoparticle real dielectric function with pressure (obtained here by modifying only $\omega_P(P)$ in the numerator of the previous formula, orange dashed line in Figure 3c). Experimental data are well reproduced by considering this additional effect, which is induced by electron density increase upon a ∼ 5% reduction of the nanoparticle volume at 10 GPa, as predicted by the bulk gold equation of state.

These investigations were repeated on several single Au-BPs with aspect ratio η ranging from 2.8 to 3.2, which presented comparable evolution of their plasmonic response (Figures 3d and S3). Comparison of individual LSPR shifts revealed a reversible spectral position upon pressure increase and release and a good reproducibility up to 4 GPa. Above this value, some spectra presented an anomalous and irreversible variation (red dots in Figures 3d and S3), probably due to shape modification[22,28,29] of the Au-BP undergoing a plastic deformation, fracture, and/or creation of defects.

CONCLUSION

We have developed a high-pressure single-nanoparticle optical spectroscopy setup by combining the high-sensitivity far-field SMS technique with an ultraflat DAC. We have performed quantitative optical measurements of the extinction spectrum of a single gold nanoparticle up to 10 GPa. Detailed comparison between experiment and theory elucidates the physical mechanisms behind the pressure tuning of its plasmonic response, in particular the disentanglement of the intrinsic (metal) and extrinsic (local environment) contributions. This opens the way to a broad spectrum of high-pressure optical investigations at the single nanoparticle level, in order to address fundamental questions like size-dependent plasmonic damping channels, nanoparticle phase transformations, equation of state, and ultrafast mechanical and thermal responses, as well as technological perspectives, including material engineering in the irreversible regime or straintronics on individual carbon nanotubes and bidimensional systems.

METHODS

Diamond Anvil Cell for High-Pressure Single-Particle Optical Spectroscopy. The anvils of the specifically designed ultraflat membrane DAC are Boehler-Almax type IIA diamonds of 1.4 mm thickness and culet diameter 0.4 mm (Figure S1). They are glued to tungsten-carbide seats having very large apertures (90° and 106° for the top and bottom parts of the cell) enabling the transmission of a tightly focused laser beam in ultraclose-field conditions. Objectives with working distances as low as 10 and 3.4 mm can be placed on the top and bottom of the DAC facing the diamond anvils, making it perfectly suited to the SMS setup. The DAC (mass 0.4 kg) is held in place by an aluminum support, yielding a total mass of 0.6 kg. The sample chamber was determined by the use of a preindented Cu−Be metallic gasket placed between the diamond anvils. A 50 μm thickness indentation with a 130 μm diameter hole (drilled by electro-erosion) was the chosen geometry in all the experiments.

High-Pressure Extinction Spectra of a Single Au-BP. Extinction spectra of individual Au-BPs spin-coated on the inner surface of one diamond anvil were first measured at room temperature and ambient pressure using the SMS technique, by tuning the incident wavelength λ. Single Au-BPs are easily distinguished from clusters or nanodusts as they present a quasi-Lorentzian spectrum with sinusoidal polarization response (Figure 2b,c).

High pressure was then achieved by loading the DAC with a 4Me:1Et mixture used as pressure-transmitting medium (ensuring hydrostatic conditions up to 10 GPa) and immediately applying an external force to avoid evaporation, resulting in a typical internal low pressure of 0.06 GPa. Pressure measurement was achieved by monitoring the R1 luminescence line of a ruby sphere (diameter of 6−8 μm) put on the inner surface of the lower anvil culet and excited by a CW laser of 532 nm wavelength.[41] To prevent contamination of SMS signals, particular attention was paid to spatially separate the ruby gauge from the investigated nanoparticles, by placing the ruby on the opposite anvil to the one with deposited nanoparticles and by maintaining >15 μm lateral distance from them. The DAC mechanical stabilization was reached after 1 h following each pressure change, before SMS characterization. Pressure drifts before and after the SMS measurements were typically 0.02 GPa (error bars in Figure 3 include these fluctuations and uncertainties related to ruby scale calibration). To study the reversibility of the optical response, spectra characterizations were performed by gently releasing the pressure in the DAC down to residual values of 1−2 GPa.

Numerical and Analytical Modeling. Complete modeling of the optical response of a Au-BP in its local environment, i.e. deposited on a diamond substrate and immersed in liquid 4Me:1Et (Figure 3a), was performed using a FEM approach.[13] This is based on the numerical computation of the electromagnetic field scattered by a Au-BP illuminated by a plane wave through the upper diamond (whose partial reflection on the diamond surface is here taken into account) in a simulation domain bounded by perfectly matched layers to avoid spurious light reflections. Absorption and scattering cross sections are then deduced from the computed field by integration of resistive heating over the Au-BP volume and of the scattered intensity through a closed surface surrounding the Au-BP, respectively. The diamond substrate and pressure-transmitting liquid were both modeled as semi-infinite media. Au-BPs were described as truncated bicones with hemispherical ends. Horizontal BP orientation with a 2 nm BP−diamond separation (because of the surfactant coating layer) was assumed, corresponding to a conformation evidenced by 3D electron tomography.[14] However, note that the predicted LSPR shifts depend weakly on the precise configuration assumed; similar results are obtained for direct BP−diamond contact or inclined BP orientation (Figure S2). The sizes of the investigated single Au-BP could not be directly retrieved by TEM imaging (the nanoparticles being deposited on the diamond anvil) but were deduced from the optical measurements[13] and in agreement with the colloidal mean sizes and dispersion. In particular, the aspect ratio of each modeled BP was obtained by fitting its SMS spectrum measured in liquid environment at the lowest pressure ($P \approx 0.06$ GPa), yielding $\eta = 3$ for the Au-BP of Figure 3.

The volume $V(P)$ of a BP compressed under high pressure at constant aspect ratio was described following the Vinet equation of state for gold, using the atmospheric pressure bulk modulus $B_0 = 167$ GPa and its pressure derivative $B_0' = 5.5$.[36] The frequency- and pressure-dependent dielectric functions of 4Me:1Et and diamond were described using available experimental data.[40] The dielectric function of Au-BPs was deduced from Johnson and Christy tables for bulk gold modified to take into account confinement effects.[3] Its pressure dependence was taken into account through modifications of the plasma frequency $\omega_P(P) = \omega_P(P_0)[V(P_0)/V(P)]^{1/2}$ governing the Drude dielectric response of the conduction electrons. In the investigated LSPR wavelength range far from interband transitions (800−950 nm), pressure-induced modification of the real interband part of the gold dielectric function is expected to provoke weaker variations of the LSPR position as compared to the dominant liquid effect: using a rigid band-shift model,[24,38] an additional LSPR spectral

DOI: 10.1021/acsnano.8b05539
ACS Nano XXXX, XXX, XXX−XXX

red-shift at 10 GPa of <1% can be estimated (smaller than the liquid and intraband contributions by more than an order of magnitude and a factor of 5, respectively, and thus neglected here). Note that the weak spectral dispersion of $\varepsilon_1^{ib}(\Omega_R(P))$ has also been neglected in the model, as it would affect only slightly the pressure-induced variations of Ω_R (<1%).

Because of the enhanced Au-BP sensitivity to liquid medium variations (due to electromagnetic field enhancement in the vicinity of its tips) and negligible pressure dependence of diamond refractive index, its optical response could then be simply modeled, in the quasi-static approximation, considering an effective prolate gold nanoellipsoid embedded in a homogeneous matrix of dielectric function $\varepsilon_l(P)$ (Figure 3b). The LSPR spectral position is then given by the analytical formula $\Omega_R(P) = \omega_P(P)/\sqrt{\tilde{\varepsilon}_1^{ib} + H\varepsilon_l(P)}$ where $\tilde{\varepsilon}_1^{ib}$ and H are pressure-independent constants. In the BP case, no analytical expression is available for the η-dependence of the geometrical factor H, in contrast to the ellipsoid one.[3] Moreover, $\tilde{\varepsilon}_1^{ib}$ is here an effective dielectric constant depending on both the interband gold real dielectric function at the resonance frequency and the diamond dielectric constant. For each BPs' aspect ratio, these two constants were thus determined at ambient pressure by FEM-computing the LSPR position of a BP deposited on diamond substrate for different liquid dielectric constants ε_l and extracted from the intercept and slope, respectively, of the linear ε_l dependence of $(\Omega_R/\omega_P)^{-2}$. For the Au-BP of Figure 2 with $\eta = 3$, this yields $H = 13$ and $\tilde{\varepsilon}_1^{ib} = 10.7$, a value slightly larger than the interband gold real dielectric function ($\tilde{\varepsilon}_1^{ib} \approx 10$ at $\lambda_R = 820$ nm), as expected. From the analytical formula, it is then easy to distinguish the pressure variations induced by the main extrinsic and intrinsic mechanisms described above. This is highlighted in Figure 3c by taking into account the change of the liquid refractive index only (i.e., $\Omega_{R,l}(P) = \omega_P(P_0)/\sqrt{\tilde{\varepsilon}_1^{ib} + H\varepsilon_l(P)}$, blue dotted line), or of the metal dielectric function only (i.e., $\Omega_{R,Au}(P) = \omega_P(P_0)/\sqrt{\tilde{\varepsilon}_1^{ib} + H\varepsilon_l(P_0)}$, orange dashed line), whose contribution is very close to the difference $\Omega_R(P) - \Omega_{R,l}(P)$.

ASSOCIATED CONTENT

Supporting Information

The Supporting Information is available free of charge on the ACS Publications website at DOI: 10.1021/acsnano.8b05539.

> Ultraflat membrane diamond anvil cell developed for SMS high-pressure experiments; influence of Au-BP deposition configuration on computed pressure-induced LSPR shifts; measured and modeled pressure dependences of the LSPR spectral positions of single Au-BPs (PDF)

AUTHOR INFORMATION

Corresponding Author

*E-mail: natalia.del-fatti@univ-lyon1.fr.

ORCID

Paolo Maioli: 0000-0002-4199-8810

Aurélien Crut: 0000-0003-2185-709X

Natalia Del Fatti: 0000-0002-8074-256X

Present Addresses

†M.H.: Research Center for Non Destructive Testing GmbH, 4040 Linz, Austria.

‡A.T.D.: CEMES, UPR-8011 CNRS, University of Toulouse, 31055 Toulouse, France.

§F.L.: Univ Lyon, CNRS, LaMCoS UMR5259, INSA-Lyon, 69621 Villeurbanne, France.

Notes

The authors declare no competing financial interest.

ACKNOWLEDGMENTS

The authors thank Luis M. Liz-Marzán, Ana Sánchez-Iglesias, and Mona Tréguer for providing us with high-quality colloidal solutions of gold nanobipyramids. This work was supported by the LABEX iMUST (ANR-10-LABX-0064) of Université de Lyon, within the program "Investissements d'Avenir" (ANR-11-IDEX-0007) operated by the French National Research Agency (ANR), and by ANR programme P2N under Contract ANR-11-NANO-025TRI-CO.

REFERENCES

(1) Kelly, K. L.; Coronado, E.; Zhao, L. L.; Schatz, G. C. The Optical Properties of Metal Nanoparticles: The Influence of Size, Shape, and Dielectric Environment. *J. Phys. Chem. B* **2003**, *107*, 668−677.

(2) Jain, P. K.; Huang, X.; El-Sayed, I. H.; El-Sayed, M. A. Review of Some Interesting Surface Plasmon Resonance-Enhanced Properties of Noble Metal Nanoparticles and Their Applications to Biosystems. *Plasmonics* **2007**, *2*, 107−118.

(3) Crut, A.; Maioli, P.; Del Fatti, N.; Vallée, F. Optical Absorption and Scattering Spectroscopies of Single Nano-Objects. *Chem. Soc. Rev.* **2014**, *43*, 3921−3956.

(4) Ringe, E.; Sharma, B.; Henry, A.-I. I.; Marks, L. D.; Van Duyne, R. P. Single Nanoparticle Plasmonics. *Phys. Chem. Chem. Phys.* **2013**, *15*, 4110−4129.

(5) Chen, H.; Kou, X.; Yang, Z.; Ni, W.; Wang, J. Shape- and Size-Dependent Refractive Index Sensitivity of Gold Nanoparticles. *Langmuir* **2008**, *24*, 5233−5237.

(6) Noguez, C. Surface Plasmons on Metal Nanoparticles: The Influence of Shape and Physical Environment. *J. Phys. Chem. C* **2007**, *111*, 3806−3819.

(7) Sun, Y.; Xia, Y.; Melillo, J. M.; Bowles, F. P.; Melillo, J. M.; Steudler, P. A.; Rayment, M.; Trumbore, S. E.; Amundson, R.; Bergh, J.; Linder, S.; Lundmark, T.; Elfving, B.; Jarvis, P.; Linder, S.; Harte, J.; Luo, Y.; Wan, S.; Hui, S.; Wallace, L.; Merriam, J.; Mcdowell, W. H.; Currie, W. S. Shape-Controlled Synthesis of Gold and Silver Nanoparticles. *Science* **2002**, *298*, 2176−2179.

(8) Grzelczak, M.; Pérez-Juste, J.; Mulvaney, P.; Liz-Marzán, L. M. Shape Control in Gold Nanoparticle Synthesis. *Chem. Soc. Rev.* **2008**, *37*, 1783−1791.

(9) Jiménez de Aberasturi, D.; Hamon, C.; Liz-Marzán, L. M. Chemical Synthesis of Plasmonic Nanoparticles. In *World Scientific Handbook of Metamaterials and Plasmonics*; Maier, S. A., Ed.; World Scientific, 2017; Vol. *4*.

(10) Crut, A.; Maioli, P.; Vallée, F.; Del Fatti, N. Linear and Ultrafast Nonlinear Plasmonics of Single Nano-Objects. *J. Phys.: Condens. Matter* **2017**, *29*, 123002.

(11) Sánchez-Iglesias, A.; Pastoriza-Santos, I.; Pérez-Juste, J.; Rodríguez-González, B.; García De Abajo, F. J.; Liz-Marzán, L. M. Synthesis and Optical Properties of Gold Nanodecahedra with Size Control. *Adv. Mater.* **2006**, *18*, 2529−2534.

(12) Sánchez-Iglesias, A.; Winckelmans, N.; Altantzis, T.; Bals, S.; Grzelczak, M.; Liz-Marzán, L. M. High-Yield Seeded Growth of Monodisperse Pentatwinned Gold Nanoparticles through Thermally Induced Seed Twinning. *J. Am. Chem. Soc.* **2017**, *139*, 107−110.

(13) Lombardi, A.; Loumaigne, M.; Crut, A.; Maioli, P.; Del Fatti, N.; Vallée, F.; Spuch-Calvar, M.; Burgin, J.; Majimel, J.; Tréguer-Delapierre, M. Surface Plasmon Resonance Properties of Single Elongated Nano-Objects: Gold Nanobipyramids and Nanorods. *Langmuir* **2012**, *28*, 9027−9033.

(14) Pertreux, E.; Lombardi, A.; Florea, I.; Spuch-Calvar, M.; Gómez-Graña, S.; Ihiawakrim, D.; Hirlimann, C.; Ersen, O.; Majimel, J.; Tréguer-Delapierre, M.; Hettich, M.; Maioli, P.; Crut, A.; Vallée, F.; Del Fatti, N. Surface Plasmon Resonance of an Individual Nano-Object on an Absorbing Substrate: Quantitative Effects of Distance and 3D Orientation. *Adv. Opt. Mater.* **2016**, *4*, 567−577.

DOI: 10.1021/acsnano.8b05539
ACS Nano XXXX, XXX, XXX−XXX

(15) Sepúlveda, B.; Angelomé, P. C.; Lechuga, L. M.; Liz-Marzán, L. M. LSPR-Based Nanobiosensors. *Nano Today* **2009**, *4*, 244−251.
(16) Burgin, J.; Liu, M.; Guyot-Sionnest, P. Dielectric Sensing with Deposited Gold Bipyramids. *J. Phys. Chem. C* **2008**, *112*, 19279−19282.
(17) San-Miguel, A. Nanomaterials under High-Pressure. *Chem. Soc. Rev.* **2006**, *35*, 876−889.
(18) Van Den Broeck, N.; Putteneers, K.; Tempere, J.; Silvera, I. F. Nanoshells as a High-Pressure Gauge Analyzed to 200 GPa. *J. Appl. Phys.* **2011**, *110*, 114318.
(19) Hohensee, G. T.; Wilson, R. B.; Cahill, D. G. Thermal Conductance of Metal−diamond Interfaces at High Pressure. *Nat. Commun.* **2015**, *6*, 6578.
(20) Li, B.; Wen, X.; Li, R.; Wang, Z.; Clem, P. G.; Fan, H. Stress-Induced Phase Transformation and Optical Coupling of Silver Nanoparticle Superlattices into Mechanically Stable Nanowires. *Nat. Commun.* **2014**, *5*, 4179.
(21) Mokkath, J. H. Strain Induced Plasmon Tuning in Planar Square-Shaped Aluminum Nanoparticles Array. *Chem. Phys. Lett.* **2018**, *702*, 102−105.
(22) Bao, Y.; Zhao, B.; Tang, X.; Hou, D.; Cai, J.; Tang, S.; Liu, J.; Wang, F.; Cui, T. Tuning Surface Plasmon Resonance by the Plastic Deformation of Au Nanoparticles within a Diamond Anvil Cell. *Appl. Phys. Lett.* **2015**, *107*, 201909.
(23) Bao, Y.; Zhao, B.; Hou, D.; Liu, J.; Wang, F.; Wang, X.; Cui, T. The Redshift of Surface Plasmon Resonance of Colloidal Gold Nanoparticles Induced by Pressure with Diamond Anvil Cell. *J. Appl. Phys.* **2014**, *115*, 223503.
(24) Christofilos, D.; Assimopoulos, S.; Del Fatti, N.; Voisin, C.; Vallée, F.; Kourouklis, G. A.; Ves, S. High Pressure Study of the Surface Plasmon Resonance in Ag Nanoparticles. *High Pressure Res.* **2003**, *23*, 23−27.
(25) Coffer, J. L.; Shapley, J. R.; Drickamer, H. G. The Effect of Pressure on the Surface Plasmon Absorption Spectra of Colloidal Gold and Silver Particles. *J. Am. Chem. Soc.* **1990**, *112*, 3736−3742.
(26) Jayaraman, A. Ultrahigh Pressures. *Rev. Sci. Instrum.* **1986**, *57*, 1013−1031.
(27) Dubrovinsky, L.; Dubrovinskaia, N.; Prakapenka, V. B.; Abakumov, A. M. Implementation of Micro-Ball Nanodiamond Anvils for High-Pressure Studies above 6 Mbar. *Nat. Commun.* **2012**, *3*, 1163.
(28) Yang, W.; Huang, X.; Harder, R.; Clark, J. N.; Robinson, I. K.; Mao, H. Coherent Diffraction Imaging of Nanoscale Strain Evolution in a Single Crystal under High Pressure. *Nat. Commun.* **2013**, *4*, 1680.
(29) Huang, X.; Yang, W.; Harder, R.; Sun, Y.; Lu, M.; Chu, Y. S.; Robinson, I. K.; Mao, H. K. Deformation Twinning of a Silver Nanocrystal under High Pressure. *Nano Lett.* **2015**, *15*, 7644−7649.
(30) Bowman, R. W.; Gibson, G. M.; Padgett, M. J.; Saglimbeni, F.; Di Leonardo, R. Optical Trapping at Gigapascal Pressures. *Phys. Rev. Lett.* **2013**, *110*, 095902.
(31) Arbouet, A.; Christofilos, D.; Del Fatti, N.; Vallée, F.; Huntzinger, J. R.; Arnaud, L.; Billaud, P.; Broyer, M. Direct Measurement of the Single-Metal-Cluster Optical Absorption. *Phys. Rev. Lett.* **2004**, *93*, 127401.
(32) Christofilos, D.; Blancon, J.-C.; Arvanitidis, J.; Miguel, A. S.; Ayari, A.; Del Fatti, N.; Vallée, F. Optical Imaging and Absolute Absorption Cross Section Measurement of Individual Nano-Objects on Opaque Substrates: Single-Wall Carbon Nanotubes on Silicon. *J. Phys. Chem. Lett.* **2012**, *3*, 1176−1181.
(33) Blancon, J.-C.; Paillet, M.; Tran, H. N.; Than, X. T.; Guebrou, S. A.; Ayari, A.; Miguel, A. S.; Phan, N.-M.; Zahab, A.-A.; Sauvajol, J.-L.; Del Fatti, N.; Vallée, F. Direct Measurement of the Absolute Absorption Spectrum of Individual Semiconducting Single-Wall Carbon Nanotubes. *Nat. Commun.* **2013**, *4*, 2542.
(34) Giblin, J.; Vietmeyer, F.; McDonald, M. P.; Kuno, M. Single Nanowire Extinction Spectroscopy. *Nano Lett.* **2011**, *11*, 3307−3311.
(35) Vella, A.; Shinde, D.; Houard, J.; Silaeva, E.; Arnoldi, L.; Blum, I.; Rigutti, L.; Pertreux, E.; Maioli, P.; Crut, A.; Del Fatti, N. Optothermal Response of a Single Silicon Nanotip. *Phys. Rev. B: Condens. Matter Mater. Phys.* **2018**, *97*, 075409.
(36) Takemura, K.; Dewaele, A. Isothermal Equation of State for Gold with a He-Pressure Medium. *Phys. Rev. B: Condens. Matter Mater. Phys.* **2008**, *78*, 104119.
(37) Gu, Q. F.; Krauss, G.; Steurer, W.; Gramm, F.; Cervellino, A. Unexpected High Stiffness of Ag and Au Nanoparticles. *Phys. Rev. Lett.* **2008**, *100*, 045502.
(38) Stoll, T.; Maioli, P.; Crut, A.; Del Fatti, N.; Vallée, F. Advances in Femto-Nano-Optics: Ultrafast Nonlinearity of Metal Nanoparticles. *Eur. Phys. J. B* **2014**, *87*, 260.
(39) Edwards, D. F.; Ochoa, E. Infrared Refractive Index of Diamond. *J. Opt. Soc. Am.* **1981**, *71*, 607−608.
(40) Eggert, J. H.; Xu, L.; Che, R.; Chen, L.; Wang, J. High Pressure Refractive Index Measurements of 4:1 Methanol:Ethanol. *J. Appl. Phys.* **1992**, *72*, 2453−2461.
(41) Mao, H. K.; Bell, P. M.; Shaner, J. W.; Steinberg, D. J. Specific Volume Measurements of Cu, Mo, Pd, and Ag and Calibration of the Ruby R 1 Fluorescence Pressure Gauge from 0.06 to 1 Mbar. *J. Appl. Phys.* **1978**, *49*, 3276−3283.

DOI: 10.1021/acsnano.8b05539
ACS Nano XXXX, XXX, XXX−XXX

Supporting Information for the paper

High-pressure Effect on the Optical Extinction of a Single Gold Nanoparticle

Fabio Medeghini, Mike Hettich, Romain Rouxel, Silvio D. Silva Santos, Sylvain Hermelin, Etienne Pertreux, Abraao Torres Dias, Franck Legrand, Paolo Maioli, Aurélien Crut, Fabrice Vallée, Alfonso San Miguel and Natalia Del Fatti*

Université de Lyon, CNRS, Université Claude Bernard Lyon 1, Institut Lumière Matière, 69622 Villeurbanne cedex, France

* Corresponding author, email: natalia.del-fatti@univ-lyon1.fr

Content:

Figure S1. Ultra-flat membrane diamond anvil cell developed for SMS high-pressure experiments.

Figure S2. Influence of Au-BP deposition configuration on computed pressure-induced LSPR shifts.

Figure S3. Measured and modeled pressure-dependences of the LSPR spectral positions of single Au-BPs.

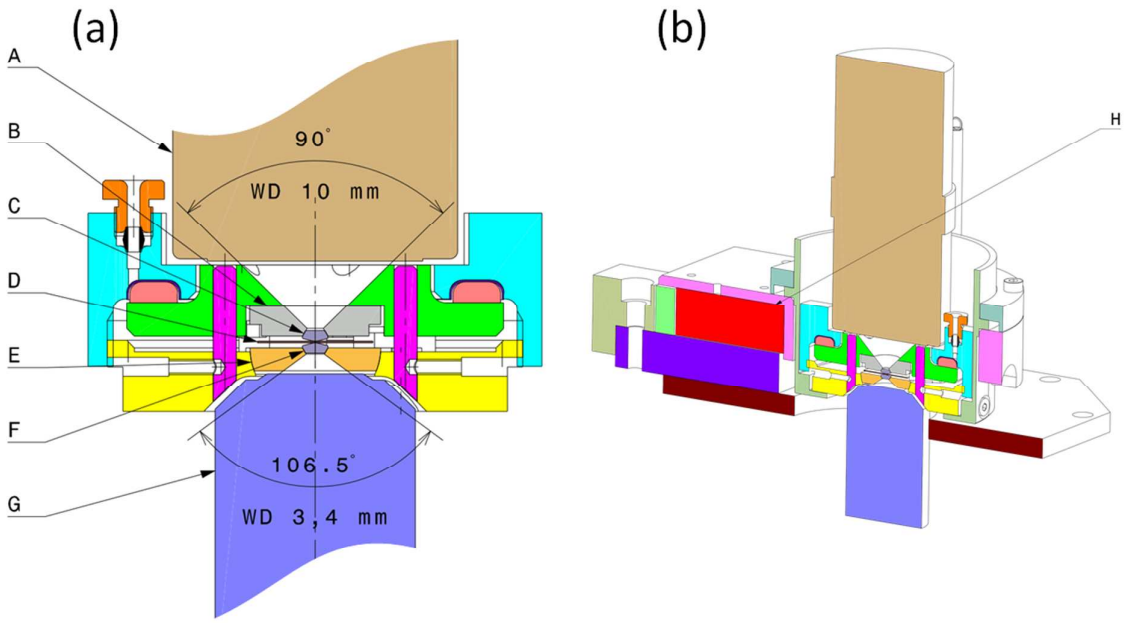

Figure S1. Ultra-flat membrane diamond anvil cell developed for SMS high-pressure experiments. **(a)** Diamond anvil cell description: the image shows a symmetric cut of the cell and associated optics. The cell body, piston and gas-membrane hood (in yellow, green and magenta colors respectively) were made on LANOX pretreated 320HB resulfurated stainless steel from Lugand, as a compromise between mechanical strength and homogeneity allowing for a very precise machining. The central part of the cell is constituted by the perforated metallic gasket (D) determining together with the two diamond anvils (C and F) the sample cavity. The two diamond anvils were supported by tungsten carbide (CW) seats (B and E). Axial alignment of the diamond anvils is made possible by the adjustments in the superior CW seat (B), whereas parallelism between the two diamond anvil culets is obtained by the tilt of the lower CW seat (E). The whole cell (≈ 5 cm diameter) was designed to allow the extreme close-up approach of two optical objectives (A and G) on both sides. Accessible working distances (WD) and optical angular aperture are both indicated in the drawing. The finite element analysis allowed to verify the correct mechanical response of the cell up to pressures of at least 10 GPa, as well as to optimize the geometry with the goal of reducing the working distance of the optical objectives. The use of conical cut diamond anvils [described in R. Boehler et al., High Press. Res. 24, 391 (2004)] participated to the reduction of the WDs. **(b)** Perspective cut of the cell inserted in the piezoelectric transducer system: the cell is tightly fixed to a support coupled to the piezoelectric linear actuator (H, in red) allowing for stable 1 kHz range oscillations between the fixed objectives.

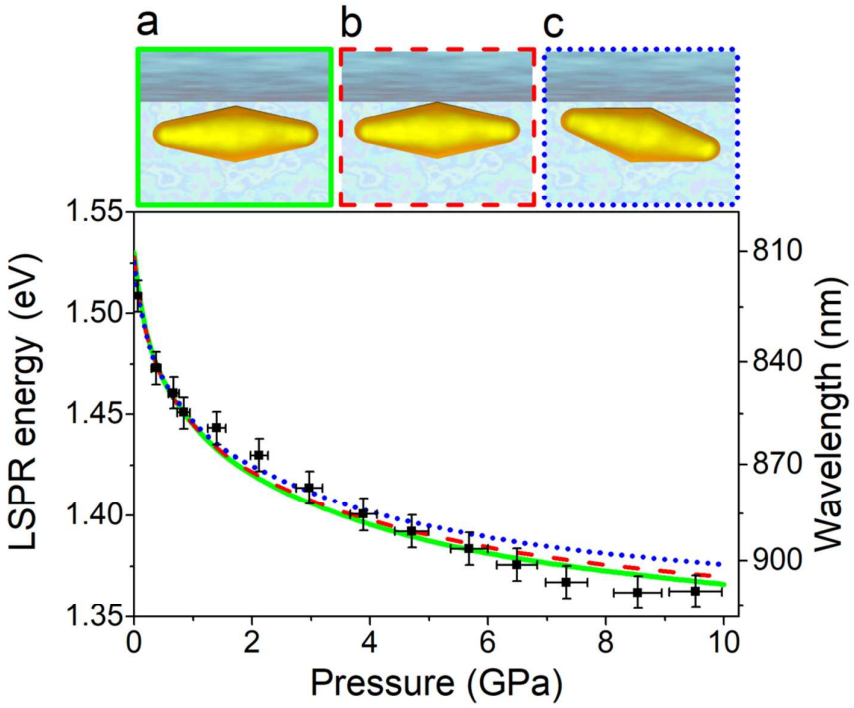

Figure S2. Influence of Au-BP deposition configuration on computed pressure-induced LSPR shifts. The figure shows the FEM-computed pressure-induced evolutions of LSPR position for three different configurations differing by BP orientation and/or distance to the diamond substrate. Experimental data (black symbols) are the same as in Fig. 3-c. Configuration **(a)** (green solid line, as in Fig. 3-c): horizontal BP orientation with 2 nm separation between the BP and the substrate (of the order of the thickness of surfactant coating layer), as experimentally observed by electron tomography for BPs deposited on a carbon substrate (see Methods in main text). Configuration **(b)** (red dashed line): horizontal BP orientation, direct contact between the BP and the diamond anvil. Configuration **(c)** (blue dotted line): maximally inclined BP orientation, with 2 nm separation between the BP and the diamond anvil. Aspect ratios η of 3.0, 2.9 and 2.8 and short axis D = 30 nm were used for configurations a, b and c, so as to reproduce the SMS spectrum measured at 0.06 GPa pressure. The figure shows that pressure-induced shifts are close for all configurations, and thus that the agreement between the experimental evolution and simulated ones is not strongly sensitive to specific geometrical assumptions made in the modeling.

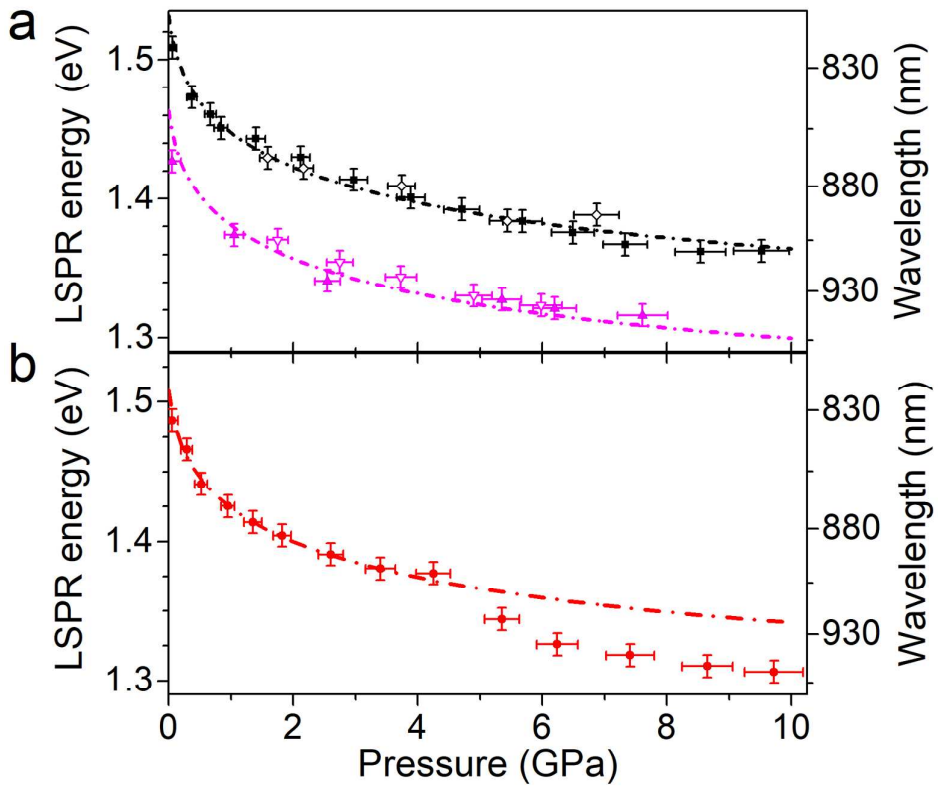

Figure S3. Measured and modeled pressure-dependences of the LSPR spectral positions of single Au-BPs. Three Au-BPs of different aspect ratio are considered (same colors as Fig. 3-d). **(a)** Measured LSPR spectral position under high pressure of two single Au-BPs with $\eta \approx 3$ (black squares) and $\eta \approx 3.2$ (magenta triangles), showing a reversible behavior upon pressure increase (solid symbols) and decrease (empty symbols), well reproduced by the analytical model (dash-dotted lines) over the 0-10 GPa pressure range. **(b)** Same information for a $\eta \approx 3$ single Au-BP (red dots) whose LSPR spectral evolution is accurately reproduced by the model (dash-dotted line) only up to 4 GPa pressure, above which a discontinuity is observed, presumably resulting from a plastic deformation of the BP and/or defect creation.